Thermal-demagnetization Analysis and Research on Physical Properties of Nd-Fe-B Sintered Magnets

Dai Higuchi
Shin-Etsu Chemical Co., Ltd.

Abstract :
Sintered Nd-Fe-B magnets are applied for many mechatronics fields but their physical properties are not sufficiently investigated. As a result, they are poorly-modeled in the simulation study.
We will therefore introduce the research results, including thermal demagnetization, electric conductivity, and thermal expansion.
Concerning thermal demagnetization, we will compare the measurement results with the JMAG analysis results.

1. Preface

Sintered Nd-Fe-B magnets are applied for many mechatronics fields but their physical properties are not sufficiently investigated. As a result, they are poorly-modeled in the simulation study.

We will therefore introduce the research results, including thermal demagnetization, electric conductivity, and thermal expansion. Concerning thermal demagnetization, we will compare the measurement results with the JMAG analysis results.

2. Electric Conductivity

This section reports the electrical resistivity (hereinafter referred to as resistivity) which is indefensible in eddy current analyses of magnets.

〈2・1〉 Anisotropy and Abnormalities of Electrical Resistivity

The resistivity component in the non-magnetization direction and magnetization direction needs to be considered when the magnetic flux does not flow perpendicularly into the magnetic pole face because eddy currents are produced in the face perpendicular to the magnetic flux.

The resistivity in the magnetization and non-magnetization directions for a sintered Nd-Fe-B magnet from Shin-Etsu is indicated in Fig. 1. The resistivity in the magnetization direction (I//M) is approximately 20% higher than the magnetization in the non-magnetization direction (I□M). The standard explanation for this is described below.

First, the anisotropy of the electric conductivity can be handled the same as single-crystal because the magnetization direction of sintered magnets are aligned. Furthermore, sparing the details, the 3D electron of Fe contributes mainly to the electric conductivity in the main phase Nd_2Fe_{14}.[1] The $Nd_2Fe_{14}B$ crystal structure [2] based on the above is indicated in Fig. 2. The characteristics of this crystal structure includes a "heavy layer of Fe" and a "layer composed of Nd, Fe, and B" which are alternately layered in the c-axis direction (magnetization direction). The resistivity is low because the electric conductivity of the ab face (non-magnetization direction) only needs electricity to pass through the "heavy layer of FE." The electric conductivity along the c-axis (magnetization direction) should have a higher resistivity than the ab face because electricity also has to pass through the "layer composed of Nd, Fe, and B."

A curve can be seen at the Curie point (Tc) indicted by the arrow in Fig. 1 for the resistivity of sintered Nd-Fe-B magnets. Materials such as metal with normal magnetic properties has resistivity that raises linearly as the temperature increases, but there is abnormal resistivity (bulge) of materials with strong magnetic properties that cannot be seen in metal resulting in a curve until the Curie point is reached. The abnormal resistivity seen below the curry point results from the mutual relationships such as the lattice constant and rate of thermal expansion.[3], [4] The distance between electrons caused by the magnetic order effects the resistivity.

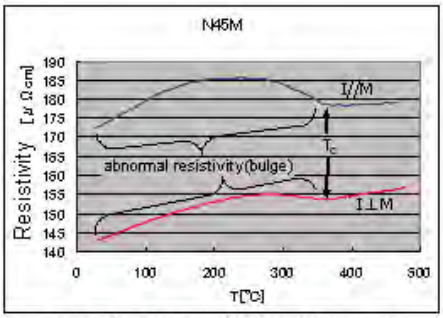

Fig. 1. Resistivity of Nd-Fe-B magnets

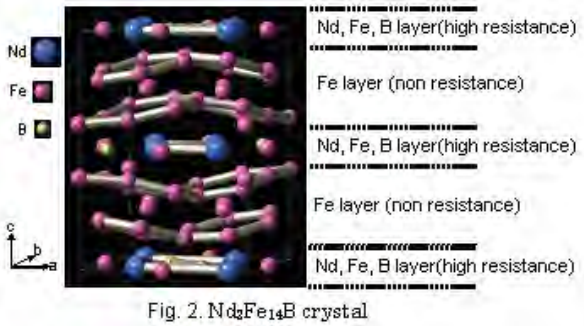

Fig. 2. $Nd_2Fe_{14}B$ crystal

〈2-2〉 Variations of Resistivity Caused by Differing Orientations

A defective orientation causes the magnetic properties in sintered magnets to worsen, but the resistivity of sintered magnets is also effected by the degree of orientation (degree crystal particles on the c-axis are aligned in the orientation direction) because the resistivity of $Nd_2Fe_{14}B$ differs in the magnetization direction and non-magnetization direction. The resistivity data of Shin-Etsu sintered magnets (oriented and non-oriented N45M) is indicated in Fig. 3. As one can assume, the resistance components along the c-axis (magnetization direction) and the resistance components along the a-axis (non-magnetization direction) mix for non-oriented magnets and the resistivity of the non-oriented magnet falls between the magnetization direction and non-magnetization direction of an oriented magnet.

The resistivity of oriented and non-oriented magnets was compared, but we can assume the resistivity will be effected in magnets that have a misaligned magnetization.

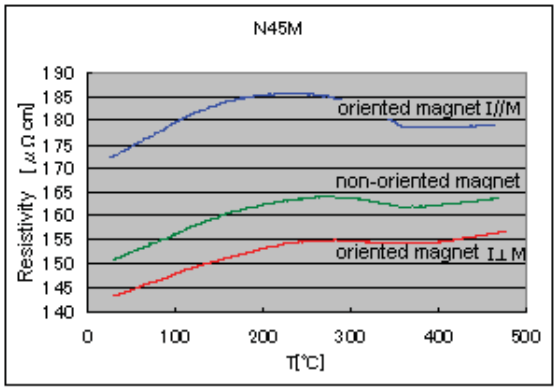

Fig. 3. Resistivity of oriented and non-oriented

3. Thermal Demagnetization of a Magnet

Magnets used in high temperature environments can suffer from irreversible demagnetization

(thermal demagnetization) caused by heat. This section describes the results of our research of thermal demagnetization. The magnet that was used is a Shin-Etsu N42SH (dimensions: 40x20x5T). The thermal demagnetization was estimated to start at 120 degrees Celsius using temperature of demagnetization obtained in a simulation of the permeance coefficient. Furthermore, the necessary Curie point used as information during thermal demagnetization is 350 degrees Celsius based on the results measuring resistance.

〈3-1〉 Repeated Thermal Demagnetization

A magnet was heated until reaching the temperature of demagnetization. This was then repeated to see whether further demagnetization would occur. The amount of flux if a fully magnetized magnet is 100% is indicated for each temperature in Fig. 5. Thermal demagnetization was repeated at each temperature, but the amount of flux did not decrease after the second time.

〈3-2〉 Thermal Demagnetization and Remagnetization

The amount of flux that could be regained after thermal demagnetization was examined by remagnetizing a magnet with thermal demagnetization using a pulse magnetizer. The magnetization field that was determined arbitrarily was 27 kOe (2.15 MA/m). Fig. 5 plots the flux after thermal demagnetization (Flux after demagnetization) at each temperature on the horizontal axis and the flux after remagnetization (Flux after remagnetization) on the vertical axis. A thermally demagnetized magnet was fully demagnetized by heating it to 400 degrees Celsius, remagnetized (flux returned to initial state), and then used to test demagnetization at a different temperature. The flux after thermal demagnetization decreases linearly as the temperature for thermal demagnetization increases. The flux after remagentization decreases linearly up to 250 degrees Celsius as the temperature rises, but then bottoms out between 250 to 270 degrees Celsius before increasing linearly at higher temperatures.

The following can be noted from the above results. Even with a magnetic field strong enough to fully magnetize a non-magnetized magnet, the magnet cannot be fully magnetized after thermal demagnetization inferring that the thermally demagnetized magnet has a magnetic domain structure that is difficult to magnetize. However, the type of magnetic domain structure is still unclear. This will be part of our future research.

The size of the remagnetization field for the testing indicated in Fig. 5 is 27 kOe (2.15 MA/m). The flux after remagentization at the lowest point of 150 degrees Celsius was able to be fully remagnetized using a magnetic field of 56 kOe (4.46 MA/m)

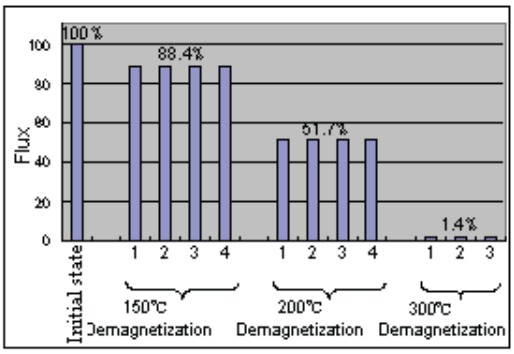

Fig. 4. Repeated

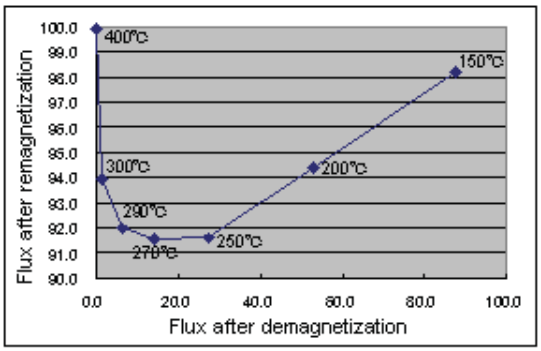

Fig. 5. Flux after thermal demagnetization

〈3-3〉 Thermal Demagnetization Region

This section reports the results from observing regions that thermal demagnetization occurs.

A map of the permeance coefficient analyzed using the electromagnetic field simulation software JMAG-Designer from the JSOL Corporation is indicated in Fig. 6. Around the center of the magnetic pole face has the lowest permeance coefficient and is where the demagnetization is occurring.

Images of the magnetic pole faces of a fully magnetized magnet and a magnet that has thermal demagnetization at 150 degrees Celsius using a magnet viewer and N42SH magnets from Shin-Etsu are indicated in Fig. 7. The magnet viewer displays regions with magnetic poles (regions with a clear N or S pole) in black and regions without poles in yellow. Multiple blotches can be seen in around the center of the magnetic pole face. These blotches are regions related to the demagnetization. The demagnetization regions do not appear in one large area, but as many tiny blotches which differs from the analysis, but, considering the whole, the demagnetization regions exist around the center which matches the analysis results. Enlarged views of the blotches around the center of the magnetic poles are indicated in Fig. 7 (c) and Fig. 7(b). The blotches are approximately 0.5 to 1 mm with black inside. The yellow region sandwiched with black on the outside of the blotch and the inside of the blotch means that the black on the inside of the blotch is a pole in the opposite direction as the magnetized. More specifically, the demagnetization regions mean the reverse magnetic domains on the surface of the magnet.

Fig. 6 Permeance

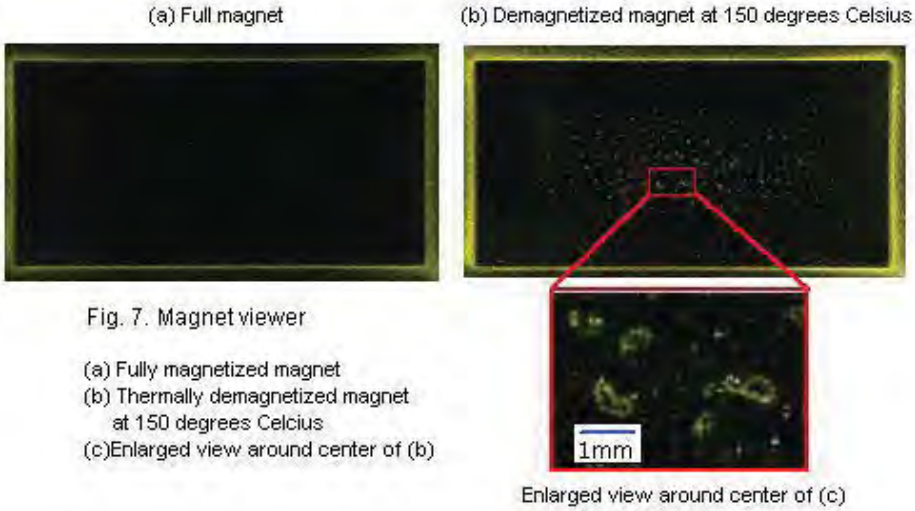

Fig. 7. Magnet viewer

(a) Fully magnetized magnet
(b) Thermally demagnetized magnet at 150 degrees Celcius
(c)Enlarged view around center of (b)

Enlarged view around center of (c)

A map measuring the magnetic flux from the magnetic pole face using a hall effect sensor for a region of 6 mm angle around the center of the magnet is indicated in Fig. 8. The hall sensor was used at a 0.7 mm distance from the magnetic pole face and a measuring pitch of 0.2 mm. Many circular regions can be seen in the 2-dimensional map. A mixture of regions with higher flux and lower flux can be seen in the 3-dimensional graph. Just as the results obtained using a magnet viewer, the results differ from the analysis results assuming a uniform demagnetization.

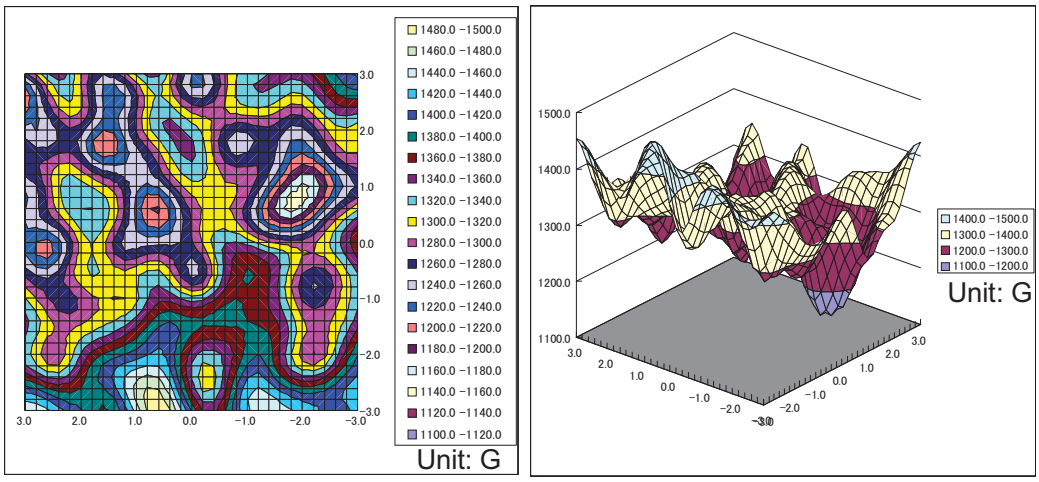

Fig. 8 Surface flux of demagnetization region (left: 2D map; right: 3D graph)

The flux that was measured is not only for the front. The results measured for the back are indicated in Fig. 9. (The horizontal axis is reversed to make comparing the flux for the front and back easier.) The fornt and back have regions that are the similar size. The demagnetization regions on the front span to the back. Even in the magnetic domain structure observed in the XMCD of a magnet demagnetized using heat after being magnetized has magnetic domain regions stretching in the magnetization direction.[5]

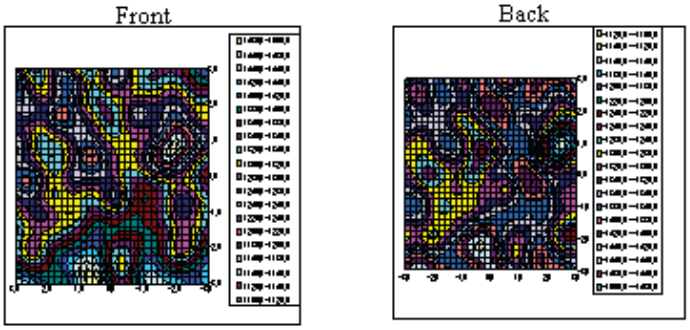

Fig. 9 Flux on the front and back of the magnet (Horizontal axis reversed for back side)

4. Thermal Demagnetization of Magnets in Motors

This section compares the actual results and results obtained using JMAG-Designer for thermal demagnetization when neodymium magnets are used in motors.

The magnets that are used are N52 grade from Shin-Etsu. This grade of magnet is used for this testing even though they are not used often in motors because their coercive force is small and they are relatively easy to thermally demagnetize. The motor used for evaluation is a 4-pole 6-slot IPM with a concentrated winding for an air compressor. The parameters of the motor used for the analysis and

testing is indicated in Table 1.

Model	4pole-6slot Concentrated Windings
Output	750W
Rotor diameter	55mm
Core material	35A300
Air Gap	0.5mm
Magnet material	N52(Br 1.44T, bHc 860kA/m)
Coil Turn	200turn/Slot

Table 1. Motor parameters for thermal demagnetization evaluation

The thermal demagnetization analysis results using JMAG and the thermal demagnetization testing results using the prototype are indicated in Fig. 10. Furthermore, the data for the magnetic properties of N52 used for the JMAG thermal demagnetization analysis are the actual values obtained with a BH curve tracer from room temperature to 200 degrees Celsius. Based on the results we obtained, The analysis and actual results match for low current regions under 8 A, but the they begin to diverge as the applied current increases. The cause of this divergence is still not completely clear, but the difference between the conventional theory of irreversible demagnetization and the actual behavior of thermal demagnetization is one primary cause.

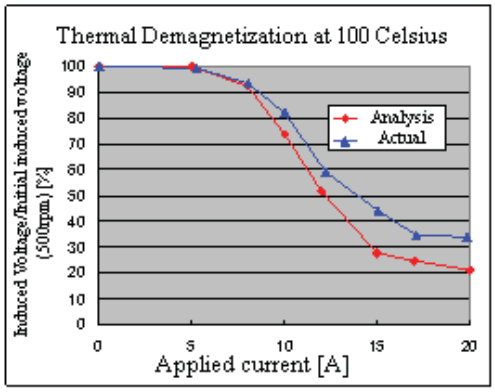

Fig. 10 Analysis and Actual

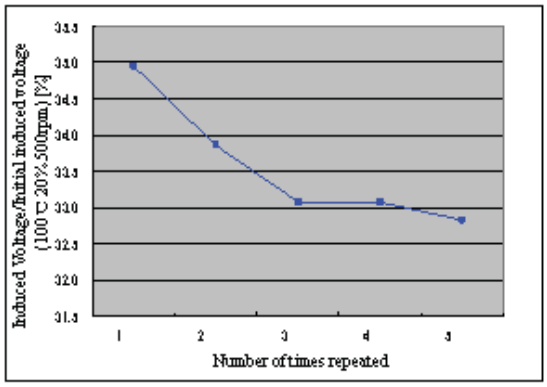

Fig. 11 Repeated

The difference in the values derived using the conventional permeance method for the initial irreversible demagnetization is minimal, but, as the demagnetization becomes large, the irreversible demagnetization is slower than the results obtained by conventional methods because the demagnetization accelerates at high temperature regions for the conventional method while the stability of the magnetic energy caused by reversed magnetic domains is contributory.

These results do not mean that we can claim that quantifying irreversible demagnetization using thermal demagnetization analysis tools is difficult. This is because the divergence in results only starts at large amounts of demagnetization and thermal demagnetization analysis of motors, etc., does

not realistically evaluate demagnetization above 10%. Therefore, analysis results using JMAG are sufficiently accurate for general applications at temperatures that irreversible demagnetization begins.

The results for the repeated demagnetization after initially testing thermal demagnetization are indicated in Fig. 11. In this analysis, a motor was heated to 100 degrees Celsius and a direct current of 20 A was applied, and then the no-load induced voltage was measured after cooling to room temperature. This is 1 time that is repeated in a continuous cycle. The results indicated a gradual reduction in the induced voltage when this process is repeated, but there is very little variation after the third time the process is undertaken. The permeance of the demagnetized magnet has continuous variations assuming the reduction in induced voltage is caused by the irreversible demagnetization in the entire magnet, but the demagnetization does not worsen after a certain point because the permeance stabilizes based on these results.

5. Conclusion

The difference between the electric conductivity in the magnetization direction and non-magnetization direction for rare earth permanent magnets differ because the crystal orientation has a phase of 2-14-1. Furthermore, as a whole the permeance distribution for the thermal demagnetization of magnets in the JMAG analysis results match the actual demagnetization. The demagnetization is composed of complicated magnetic domains because of the microscopic grain distribution that occurs. In addition, the flux distribution after demagnetization is similar on the front and back of the magnet indicating a relationship between the demagnetization on the front and back of the magnet.

The magnet demagnetized under the Curie point cannot be easily remagnetized based on the remagnetization testing after thermal demagnetization. The coercive force of the crystal particles with reversed magnetization need to have a stronger magnetic field applied to completely remagnetize the magnet because these crystal particles have reversed in a magnet that demagnetization.

Thermal demagnetization analysis using JMAG can be used as general demagnetization evaluation tool because the results match actual measurements at initial demagnetization but the results diverge from the actual measurements as irreversible demagnetization increases Furthermore,Variations in the magnet could not be seen in the repeated demagnetization testing, but, even though it was minimal, the motor showed a reduction in induced voltage Further testing and experimentation for consistency in anlayses is necessary because this phenomenon could not be examined in a thermal electromagnetic field analysis using JMAG.

Reference

（1） W.Y. Ching and Zong-Quan Gu：“Electronic structure of $Nd_2Fe_{14}B$”, J. Appl. Phys., Vol.61, No.8, pp.3718-3720 (1987).

（2） J.F. Herbst, J.J. Croat, F.E. Pinkerton, and W.B. Yelon：“Relationships between crystal structure and magnetic properties in $Nd_2Fe_{14}B$”, Phys. Rev. B, Vol.29, No.7, pp.4176-4178 (1984).

（3） A. V. Andreev, A. V. Deryagin, S.M. Zadvorkin, and S. V. Terent'ev：“Thermal expansion and spontaneous magnetostriction of $R_2Fe_{14}B$ compounds (R=Y, Nd, Sm)”, Sov. Phys. Solid State, Vol.27, No.6, pp.987-990 (1985).

（4） H. Fujii, H. Nagata, Y. Uwatoko, T. Okamoto, H. Yamamoto, and M. Sagawa：“Heat Capacity and Thermal expansion of $R_2Fe_{14}B$ compounds (R=Y, Nd and Tm)”, J. Magn. Magn. Mat., Vol.70, pp.331-333 (1987).

（5） Hiroshi Nozaki: SPring-8 Experiment Report、No. 2007A1884